Joint TOA and AOA Estimation for UWB Localization Applications

L. Taponecco, A.A. D'Amico, and U. Mengali, *Life Fellow, IEEE*

***Abstract*—A joint TOA/AOA estimator is proposed for UWB indoor ranging under LOS operating conditions. The estimator employs an array of antennas, each feeding a demodulator consisting in a squarer and a low-pass filter. Signal samples taken at Nyquist rate at the filter outputs are processed to produce TOA and AOA estimates. Performance is assessed with transmitted pulses with a bandwidth of either 1.5 GHz (type-1 pulses) or 0.5 GHz (type-2 pulses), which correspond to sampling rates of 3 GHz and 1 GHz, respectively. As expected, the estimation accuracy decreases with the pulse bandwidth. Ranging errors of about 10 cm and angular errors of about 1° are achieved at SNR of practical interest with type-1 pulses and two antennas at a distance of 50 cm. With type-2 pulses the errors increase to 35 cm and 3°. Comparisons are made with other schemes discussed in literature.**

***Index Terms*—AOA estimation, TOA estimation, UWB localization applications.**

I. Introduction

INDOOR geolocation has attracted much attention in the last few years in view of its applications in scientific, commercial and military areas [1]–[6]. An important role in this context is played by positioning systems that employ impulse radio ultra-wideband (IR-UWB) signals to perform time-of-arrival (TOA) and/or angle-of-arrival (AOA) measurements [7]–[14]. For two-dimensional positioning, three base stations (BSs) endowed with TOA measuring devices can accurately locate a mobile station (MS) if the links between the MS and BSs are in line-of-sight (LOS). The BSs can be reduced to two if AOA instead of TOA devices are used [15]–[18]. Just one BS is sufficient if both TOA and AOA measurements are performed in a single device.

In a UWB indoor environment the localization problems are complicated by non line-of-sight (NLOS) propagation. Indeed, if the direct path from MS to BS is blocked by thick walls or metallic obstacles, then a path with a longer propagation delay and a different propagation direction is taken as the direct path and this results in large range/angular errors. Thus, zones may exist within the operating area where extra BSs must be used in order to achieve adequate localization accuracy [19]–[21].

The amount of extra BSs needed depends on the service area layout. In a residential environment, for example, the internal walls may be so thick that the BSs in a given room would not function outside that room. In an office environment, on the other hand, the partitionings are generally thin and large rooms (laboratories) often exist where LOS propagation is likely to occur. The same is true in warehouses where stored assets must be located with high precision. Range measurements in excess of 60 m have been demonstrated through as many as ten commercial-grade walls [22].

In this paper we are concerned with IR-UWB localization in relatively large LOS environments making use of simultaneous TOA and AOA measurements. Unfortunately, very little has been published so far on TOA/AOA positioning systems. One apparent reason for this, is their implementation complexity as they require arrays of antennas. Another reason is that while even relatively simple receivers can measure TOA with high accuracy, it is much more complex to have precise AOA measurements. In [23], [24] the authors derive the Cramer-Rao bound (CRB) for TOA and AOA estimates and show that, with a practical number of antennas, the estimation accuracy achievable with TOA is much better than with AOA. In [25] a data fusion architecture is presented, which combines TOA/AOA measurements for position estimates with enhanced accuracy, while [26]–[28] deal with the TOA/AOA estimation problem. Note that references [25]–[28] all refer to outdoor cellular systems where localization has different features to those of indoor environments.

To the best of our knowledge the only references addressing indoor UWB localization through TOA and AOA estimates are [29], [30]. The scheme proposed in [29] is very simple: each receiving antenna measures its distance from the MS and the AOA is computed through trigonometric rules. Thus, TOA and AOA are estimated separately. On the contrary, the authors in [30] describe a joint TOA/AOA measuring scheme based on the best linear unbiased estimation criterion. The resulting TOA accuracy is very good while the AOA measurements are rather coarse for most applications.

In the present paper we develop a three-step algorithm for the joint measurement of TOA and AOA. The first step gets the TOAs at the various antenna elements. The second collects the previous results and derives a joint estimate of AOA and TOA at the first antenna. The third improves the AOA estimate. The first step is rather conventional as it exploits a simple threshold crossing method discussed in [8], [9]. However, the other steps are innovative and are our major contribution.

The rest of the paper has the following outline. Signal model and receiver structure are described in the next section. Section III deals with the TOA/AOA estimator. Simulation results and comparisons are illustrated in Section IV. Closing comments follow in Section V.

Manuscript received June 3, 2010; revised December 13, 2010 and February 18, 2011; accepted March 28, 2011. The associate editor coordinating the review of this paper and approving it for publication was S. Ghassemzadeh.

The authors are with the Department of Information Engineering, University of Pisa, Via G. Caruso, 16 Pisa 56122, Italy (e-mail: {antonio.damico, umberto.mengali,lorenzo.taponecco}@iet.unipi.it).

Digital Object Identifier 10.1109/TWC.2011.042211.100966

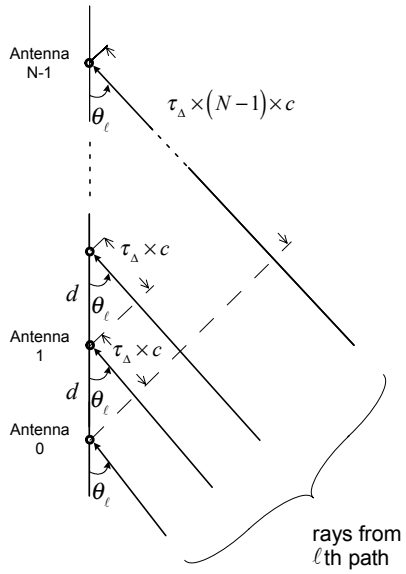

Fig. 1. Array geometry.

II. Signal model

The MS transmits the signal

$$s(t) = \sum_{i=-\infty}^{\infty} a_i w(t - iT_s) \tag{1}$$

where $w(t)$ is an ultra-short monocycle of duration T_w, $1/T_s$ is the pulse rate, and $\{a_i\}$ are independent binary data symbols taking values ± 1. Signal $s(t)$ propagates through an L-path fading channel and arrives at a uniform linear array of N antennas. Let

$$\sum_{\ell=0}^{L-1} p_\ell(t - \tau_{\ell,n}) \tag{2}$$

be the channel response to $w(t)$ at the nth antenna, where $p_\ell(t)$ is the pulse from the ℓth path and $\tau_{\ell,n}$ is the corresponding delay. In writing (2) we implicitly assume that $p_\ell(t)$ is independent of index n. This is an approximation since, in reality, the distance to the transmitter varies with n. We shall return to this point in Section III-B. Calling θ_ℓ the angle-of-arrival associated to the ℓth path and modelling the rays corresponding to a given path as parallel lines[1], from Fig. 1 we get

$$\tau_{\ell,n} = \tau_{\ell,0} + n\tau_\Delta^{(\ell)} \qquad n = 0, ..., N-1 \tag{3}$$

where $\tau_{\ell,0}$ is the time-of-arrival of the ℓth path at the first antenna,

$$\tau_\Delta^{(\ell)} = \frac{d}{c}\cos\theta_\ell \qquad \ell = 0, ..., L-1 \tag{4}$$

is the (spatial) differential delay for the ℓth path, c is the speed of light, and d the distance between two adjacent elements of the array. As we are interested in estimating the delay $\tau_{0,0}$ of the first path in arriving at the first antenna and the corresponding angle θ_0, to ease the notations we define

[1]This is the so-called far-field assumption and implies that transmitter and receiver are sufficiently far apart.

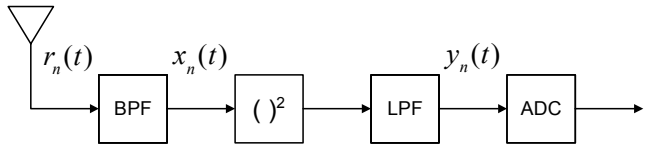

Fig. 2. Receiver's block diagram at the nth antenna.

$\rho(t) \triangleq p_0(t)$, $\tau \triangleq \tau_{0,0}$, $\tau_\Delta \triangleq \tau_\Delta^{(0)}$, $\tau_n \triangleq \tau_{0,n}$ and $\theta \triangleq \theta_0$. Accordingly (3)–(4) become

$$\tau_n = \tau + n\tau_\Delta \qquad n = 0, ..., N-1 \tag{5}$$

and

$$\tau_\Delta = \frac{d}{c}\cos\theta \tag{6}$$

The received waveform at the nth antenna can be written as

$$r_n(t) = \sum_{i=-\infty}^{\infty} a_i \left[\rho(t - \tau - n\tau_\Delta - iT_s) + \rho_n'(t - iT_s)\right] + n_n(t) \tag{7}$$

where $\rho_n'(t) \triangleq \sum_{\ell=1}^{L-1} p_\ell(t - \tau_{\ell,n})$ is the contribution of the rays arriving after the first and $n_n(t)$ is thermal noise with two-sided power spectral density $N_0/2$. The receiver's block diagram for the nth antenna is sketched in Fig. 2. As we can see, $r_n(t)$ is first passed through a band-pass filter (BPF) with center frequency f_0 and is then demodulated in a square-law device followed by a low-pass filter (LPF).

Our goal consists in measuring τ (TOA estimation) and τ_Δ, from which θ can be obtained by inverting (6) (AOA estimation). In doing so we exploit the signals $\{y_n(t)\}$ at the output of the LPFs. As we shall soon see, $y_n(t)$ can be expressed in terms of the BPF output

$$x_n(t) = \sum_{i=-\infty}^{\infty} a_i \left[q(t - \tau - n\tau_\Delta - iT_s) + q_n'(t - iT_s)\right] + n_{x_n}(t) \tag{8}$$

where $q(t)$ and $q_n'(t)$ are the convolution of $\rho(t)$ and $\rho_n'(t)$ with the BPF impulse response and $n_{x_n}(t)$ is band-pass thermal noise. To underline the band-pass nature of $x_n(t)$ we express it as a function of its complex envelope $\breve{x}_n(t)$

$$x_n(t) = \mathrm{Re}\{\breve{x}_n(t)e^{j\omega_0 t}\} \tag{9}$$

$\omega_0 \triangleq 2\pi f_0$ being the BPF central radian frequency. From (8)-(9) we find (10), where $\breve{q}(t)$, $\breve{q}'_n(t)$ and $\breve{n}_{x_n}(t)$ are the complex envelopes of $q(t)$, $q_n'(t)$ and $n_{x_n}(t)$, respectively.

The expression of $y_n(t)$ is obtained by squaring (9) and filtering in the LPF. Taking an LPF with a rectangular transfer function so that $|\breve{x}_n(t)|^2$ is passed undistorted we get

$$y_n(t) = |\breve{x}_n(t)|^2 = s_{y_n}(t) + n_{y_n}(t) \tag{11}$$

with

$$s_{y_n}(t) \triangleq |\breve{s}_{x_n}(t)|^2 \tag{12}$$

$$n_{y_n}(t) \triangleq \left[|\breve{n}_{x_n}(t)|^2 + 2\mathrm{Re}\{\breve{s}_{x_n}(t)\breve{n}_{x_n}^*(t)\}\right] \tag{13}$$

and $\breve{n}_{x_n}^*(t)$ is the complex conjugate of $\breve{n}_{x_n}(t)$.

Next we make two assumptions: (*i*) the time delay between

$$\breve{x}_n(t) = \underbrace{\sum_{i=-\infty}^{\infty} a_i[\breve{q}(t-\tau-n\tau_\Delta-iT_s)e^{-j\omega_0(\tau+n\tau_\Delta+iT_s)} + \breve{q}'_n(t-iT_s)e^{-j\omega_0 iT_s}]}_{\breve{s}_{x_n}(t)} + \breve{n}_{x_n}(t) \tag{10}$$

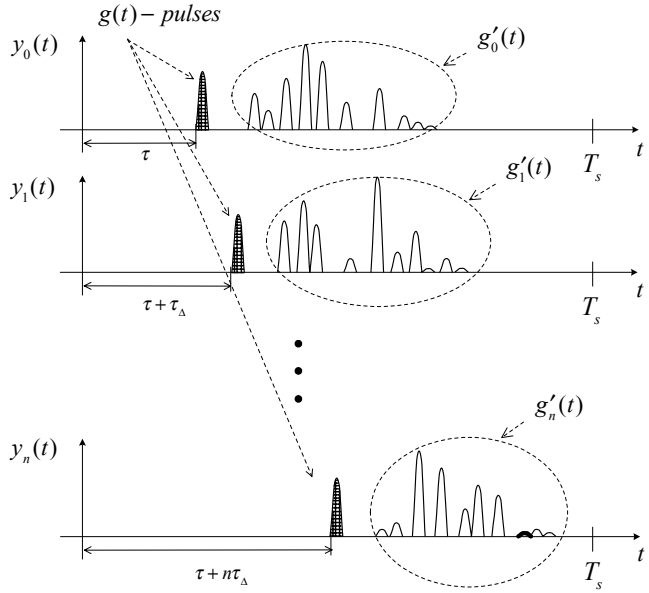

Fig. 3. Waveforms $y_n(t)$ in the absence of noise.

the first and last path at a given antenna is less than T_s; (*ii*) the first path is resolvable. Assumption (*i*) is rather mild as we are concerned with low data rates [6], say between 1 kbit/s and 1 Mbit/s. Assumption (*ii*) instead is questionable and is not always met in practice. Indeed, in some channel realizations the pulses via secondary paths overlap with that of the first path. For a given channel model the overlap occurrence depends on the signal bandwidth. With a relatively narrow bandwidth the received pulses are long and tend to merge, thus losing their distinctiveness. With a wider bandwidth, on the contrary, the pulses are shorter and their resolution is easier. In either case, in the following we keep this assumption for the sake of convenience, as it paves the way to a relatively simple TOA/AOA estimation scheme. Its effectiveness in a realistic environment is checked in Section IV.

Using the above hypotheses from (10)-(12) we get

$$y_n(t) = \sum_{i=-\infty}^{\infty} [g(t-\tau-n\tau_\Delta-iT_s) + g'_n(t-iT_s)] + n_{y_n}(t) \tag{14}$$

where $g(t) \triangleq |\breve{q}(t)|^2$ and $g_n(t) \triangleq |\breve{q}'_n(t)|^2$. Note that the a_i do not appear in (14) as they are wiped out by the action of the square-law device.

Fig. 3 shows a T_s-long segment of $y_n(t)$ in the absence of noise. The shape of the first pulse is the same at each antenna (only its delay depends on index n). On the contrary, the shape of the interfering signal $g'_n(t)$ does vary with n on account of the delays $\tau_{\ell,n}$.

III. TOA AND AOA ESTIMATION

The estimation of the propagation delay τ and of the angle-of-arrival θ is carried out with a multi-step procedure. The first step gives a measurement $\hat{\tau}_n$ of τ_n at each antenna. The second produces a joint estimate $(\hat{\tau}, \hat{\tau}_\Delta)$ of (τ, τ_Δ) making use of the previous $\hat{\tau}_n$. The third and last step provides a refinement $\hat{\hat{\tau}}_\Delta$ of $\hat{\tau}_\Delta$. Finally, an estimate of θ is derived by inverting (6) and replacing τ_Δ with $\hat{\hat{\tau}}_\Delta$.

A. Estimation of τ_n

The estimation of $\tau_n = \tau + n\tau_\Delta$ is performed with a threshold-based algorithm that provides the arrival time of the $g(t)$-pulse at the nth antenna (see Fig. 3). To begin with, we fold $y_n(t)$ K times with period T_s to produce

$$y^{(n)}_{fold}(t) = \frac{1}{K}\sum_{k=0}^{K-1} y_n(t+kT_s) \tag{15}$$

or, using (14) and assuming $\tau_n < T_s$,

$$y^{(n)}_{fold}(t) = g(t-\tau-n\tau_\Delta) + g'_n(t) + \bar{n}_{y_n}(t) \qquad 0 \le t < T_s \tag{16}$$

where

$$\bar{n}_{y_n}(t) = \frac{1}{K}\sum_{k=0}^{K-1} n_{y_n}(t+kT_s) \tag{17}$$

is a random process with mean value σ^2/K and σ^2 is the noise power at the BPF output. In practice σ^2 can be derived off-line by measuring the average of $y^{(n)}(t)$ in between signal frames. Next, following [8] we look for the first crossing of $y^{(n)}_{fold}(t)$ through a threshold λ. In practice this is done in digital form by sampling $y^{(n)}_{fold}(t)$ at Nyquist rate $1/T_N$ (twice the LPF bandwidth in Fig. 2). Assuming T_s/T_N equal to an integer M_s, the samples $y_n(\ell T_N)$ are compared with λ (the same for all the antennas) and the index of the first crossing is computed

$$\hat{\ell}_n = \min_{0\le\ell\le M_s-1}\left\{y^{(n)}_{fold}(\ell T_N) > \lambda\right\} \tag{18}$$

Then, parameter τ_n is estimated as

$$\hat{\tau}_n = (\hat{\ell}_n - 1/2)T_N \tag{19}$$

As can be imagined, the threshold value has an impact on the estimation performance. This problem is discussed thoroughly in [9] where the optimal threshold setting is found as a function of the channel statistics and the system parameters. One important result in [9] is that λ is approximately optimal when the early detection probability P_{ED} is sufficiently small for there to be little chance of noise-induced threshold crossings before the signal arrival[2]. In addition, a formula is given relating P_{ED} to the probability q_{noise} that a

[2]However P_{ED} must not be too small, since otherwise λ would be too high and would not be crossed by the arriving signal.

sample $y_{fold}^{(n)}(\ell T_N)$ exceeds λ in the absence of signal. This formula indicates that, for a given *a priori* uncertainty on the signal arrival time, P_{ED} decreases as q_{noise} gets smaller. Thus, P_{ED} may be made adequately small by setting a limit to q_{noise}. With the system parameters described in Section IV, by simulation we have found that the best TOA estimation performance is achieved when q_{noise} is in the order of 10^{-7}.

The probability q_{noise} is computed as follows. Setting $\breve{s}_{x_n}(t) = 0$ in (11) and (13) and collecting the results yields $y_n(t) = |\breve{n}_{x_n}(t)|^2$. Then, substituting into (15) and sampling gives

$$y_{fold}^{(n)}(\ell T_N) = \frac{1}{K}\sum_{k=0}^{K-1} |\breve{n}_{x_n}(\ell T_N + kT_s)|^2 \qquad (20)$$

The right hand side is the sum of K random variables (RVs), each with mean value $2\sigma^2/K$ and two degrees of freedom (since $\breve{n}_{x_n}(\ell T_N + kT_s)$ is a Gaussian random variable with circular symmetry). Taking these variables as independent, the right hand side of (20) has a chi-square distribution with $2K$ degrees of freedom and mean value $2\sigma^2$. It follows [31]

$$q_{noise} = \exp\left(-\frac{\lambda K}{2\sigma^2}\right)\sum_{k=0}^{K-1}\frac{1}{k!}\left(\frac{\lambda K}{2\sigma^2}\right)^k \qquad (21)$$

from which λ is computed by setting the right hand side (RHS) equal to 10^{-7}.

B. Estimation of τ and τ_Δ

The estimation of τ and τ_Δ is based on the following linear model of $\hat{\tau}_n$ as a function of τ_n

$$\hat{\tau}_n = \tau_n + b + \delta_n \qquad n = 0, \ldots, N-1 \qquad (22)$$

where b represents a bias and $\{\delta_n\}$ are independent, zero-mean RVs. The physical origin of b is understood with the aid of Fig. 4, which shows $y_{fold}^{(n)}(t)$ starting at $t = \tau_n$ (thermal noise is ignored but is quickly reestablished). It is seen that the threshold crossing occurs after τ_n. Computer simulations indicate that, for a given channel, the difference $\hat{\ell}_n T_N - \tau_n$ may be approximated as

$$\hat{\ell} T_N - \tau_n = b + u_n' \qquad (23)$$

where b is a positive quantity that decreases with the threshold level while u_n' accounts for the discrete-time nature of the signal samples and is uniformly distributed on $[0, T_N)$. In principle b depends on index n since the received signal strength is different at the various antennas. However it turns out that the differences between the b_n are very small fractions of the transmitted pulse duration and can be neglected. As for the effects of thermal noise, they may be accounted for by introducing in (23) an additional disturbance term $\delta_{th,n}$

$$\hat{\ell} T_N = \tau_n + b + u_n' + \delta_{th,n} \qquad (24)$$

Then, subtracting $T_N/2$ from both side of (24) and bearing in mind (19) yields

$$\hat{\tau}_n = \tau_n + b + u_n + \delta_{th,n} \qquad (25)$$

where $u_n \triangleq u_n' - T_N/2$ is uniformly distributed on $[-T_N/2, T_N/2)$. Equation (25) coincides with (22) letting

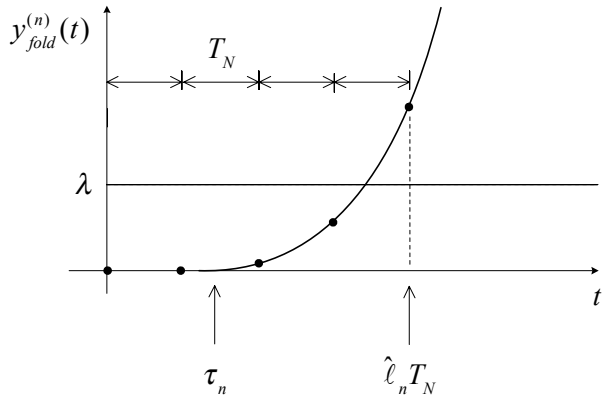

Fig. 4. Explaining the bias in the estimate of τ_n.

$\delta_n \triangleq u_n + \delta_{th,n}$. Note that, taking u_n and $\delta_{th,n}$ as independent, the variance of δ_n becomes

$$\sigma_\delta^2 = \sigma_u^2 + \sigma_{th}^2 \qquad (26)$$

where $\sigma_u^2 = T_N^2/12$, and σ_{th}^2 depends on the signal-to-noise ratio.

With the help of (22) we now address the estimation of τ and τ_Δ. Substituting (5) into (22) yields

$$\hat{\tau}_n = \tau + b + n\tau_\Delta + \delta_n \qquad n = 0, \ldots, N-1 \qquad (27)$$

which shows that $\hat{\tau}_n$ depends on three parameters: τ, b and τ_Δ. Note that, as the first two contribute to $\hat{\tau}_n$ through their sum, they cannot be estimated separately. We can either estimate $\tau + b$ or concentrate on a single addend, say τ, leaving b as an unknown quantity. We have chosen this second route and make use of least squares (LS) methods [32]. In essence we minimize the cost function

$$J(\tau, \tau_\Delta) = \sum_{n=0}^{N-1}(\hat{\tau}_n - \tau - n\tau_\Delta)^2 \qquad (28)$$

with respect to τ and τ_Δ. Skipping the details we get

$$\hat{\tau} = \frac{2}{N(N+1)}\sum_{n=0}^{N-1}\big[(2N-1) - 3n\big]\hat{\tau}_n \qquad (29)$$

$$\hat{\tau}_\Delta = \frac{12}{N(N^2-1)}\sum_{n=0}^{N-1}\left(n - \frac{N-1}{2}\right)\hat{\tau}_n \qquad (30)$$

A few remarks are useful:

1) As can be readily checked, the mean value of $\hat{\tau}$ is $\tau + b$. Thus, $\hat{\tau}$ is a biased estimator. The amount of bias is estimated to be a fraction of the $g(t)$-pulse duration in Fig. 3.
2) The mean value of $\hat{\tau}_\Delta$ is found to be τ_Δ. Thus, contrary to $\hat{\tau}$, the differential delay estimator is unbiased.
3) Straightforward calculations show that the mean-square values of the errors $\hat{\tau} - \tau$ and $\hat{\tau}_\Delta - \tau_\Delta$ are

$$\mathrm{MSE}_\tau = \frac{2(2N-1)}{N(N+1)}\sigma_\delta^2 + b^2 \qquad (31)$$

$$\mathrm{MSE}_{\tau_\Delta} = \frac{12}{N(N^2-1)}\sigma_\delta^2 \qquad (32)$$

4) At SNRs of practical interest (around 20–30 dB) and

with ADCs operating at Nyquist rate, it is experimentally found that the second term in (31) is much larger than the first. This means that the accuracy of the TOA estimates is limited by the bias and is independent of the number of antennas (it only depends on SNR on account of b).

5) In the same range of SNR values it turns out that σ_u^2 dominates over σ_{th}^2 in (26). Thus (32) becomes

$$\mathrm{MSE}_{\tau_\Delta} \cong \frac{T_N^2}{N(N^2-1)} \tag{33}$$

which says that $\mathrm{MSE}_{\tau_\Delta}$ is reduced by increasing the number of antennas.

6) Errors in the estimation of τ_Δ translate into AOA errors. Indeed, inverting (6) and replacing τ_Δ with $\hat{\tau}_\Delta$ yields

$$\hat{\theta} = \arccos(c\,\hat{\tau}_\Delta/d) \tag{34}$$

from which, assuming θ is uniformly distributed between θ_1 and θ_2, the mean-square value of $\hat{\theta}-\theta$ is found to be (see Appendix A)

$$\mathrm{MSE}_\theta = \frac{c^2}{d^2} \times \frac{1}{(\theta_2-\theta_1)}\left[\frac{1}{\tan\theta_1} - \frac{1}{\tan\theta_2}\right] \times \mathrm{MSE}_{\tau_\Delta} \tag{35}$$

For instance, taking $N=2$, $T_N = 1/3$ ns, $d = 25$ cm, $\theta_1 = 45°$ and $\theta_2 = 135°$, we have $\sqrt{\mathrm{MSE}_\theta} \cong 10°$. Observe that an error on θ produces a *transversal* error[3] of $D\,(\hat{\theta}-\theta)$ in the MS location, where D is the MS-to-BS distance. Thus, for $\hat{\theta}-\theta = 10°$ and $D = 20$ m, the tangential error is about 3.5 m, which is too large for many high-precision indoor applications.

7) Errors in the estimation of τ translate into *radial* errors $c(\hat{\tau}-\tau)$ in the MS location. For example, if the transmitted pulses have a duration of 3 ns, we expect a bias b in the order of 1 ns. On the other hand from point 4) we have $\hat{\tau}-\tau \approx b$ which corresponds to radial errors of about 30 cm.

8) The last two points indicate that, while the τ-estimator is more than satisfactory, the τ_Δ-estimator needs to be improved. This issue is addressed in the next section.

C. Improved estimation of τ_Δ

Returning to (16) it is worth remembering that $g_n'(t)$ represents the contribution of pulses arriving after $g(t-\tau-n\tau_\Delta)$. Thus, as $g(t-\tau-n\tau_\Delta)$ and $g_n'(t)$ are assumed separated in time, the latter is zero on some restricted interval around $t = \tau + n\tau_\Delta$ and we have

$$y_{fold}^{(n)}(t) = g\,(t-\tau-n\tau_\Delta) + \bar{n}_{y_n}(t) \qquad n = 0,1,...,N-1 \tag{36}$$

or equivalently, letting $z_n(t) \triangleq y_{fold}^{(n)}(t) - \sigma^2/K$,

$$z_n(t) = g(t-\tau-n\tau_\Delta) + \nu_n(t) \qquad n = 0,1,...,N-1 \tag{37}$$

where $\nu_n(t) \triangleq \bar{n}_{y_n}(t) - \sigma^2/K$ is a zero-mean noise term. In the following we take $\hat{\tau}$ as a good approximation of τ so that (37) may be rewritten

$$z_n(t) = g(t-\hat{\tau}-n\tau_\Delta) + \nu_n(t) \qquad n = 0,1,...,N-1 \tag{38}$$

[3]The location error may be divided into two components: one in the direction MS-to-BS (*radial* error), the other in the direction orthogonal to MS-to-BS (*transversal* error).

Before discussing how to improve $\hat{\tau}_\Delta$ it is worth mentioning a method described in [33] to estimate τ_Δ in room acoustic environments. The signal model in [33] is formally identical to (38) except that time t is not restricted around $\hat{\tau}+n\tau_\Delta$. This is because reference [33] assumes a single-path channel and, in consequence, $g_n'(t)$ is null and (38) holds at any time. The method in [33] is easily described in the case of two antennas and consists in maximizing the cross-correlation $C(\tilde{\tau}_\Delta) = E\{z_0(t+\tilde{\tau}_\Delta)z_1(t)\}$, where $E\{\cdot\}$ stands for mathematical expectation and $\tilde{\tau}_\Delta$ is a tentative value of τ_Δ. No limitations on the range of $\tilde{\tau}_\Delta$ are imposed. Clearly, we cannot apply this method to our problem. Indeed, in the absence of restrictions on $\tilde{\tau}_\Delta$, the cross-correlation would involve the pulses arriving after the direct path and the maximization would lead to poor results. The following approach indicates how the restrictions $\tilde{\tau}_\Delta$ can be established.

The basic idea stems from the observation of (38). If τ_Δ were known, shifting $z_n(t)$ leftward by $\hat{\tau}+n\tau_\Delta$ would produce $g(t)$ plus noise. Hence, in the summation

$$z(t;\hat{\tau},\tau_\Delta) \triangleq \frac{1}{N}\sum_{n=0}^{N-1} z_n(t+\hat{\tau}+n\tau_\Delta) \tag{39}$$

the signal components would add coherently to form $g(t)$ while the noise components would add incoherently and their overall level would be reduced. Figure 5 illustrates a possible form of $g(t)$, with T_g indicating the pulse duration (approximately equal to that of the transmitted pulses) and W_g the root-mean-square pulse width

$$W_g \triangleq \sqrt{\int_0^{T_g}(t-t_{cg})^2 g^2(t)dt \Big/ \int_0^{T_g} g^2(t)dt} \tag{40}$$

where t_{cg} is the pulse center of gravity

$$t_{cg} = \int_0^{T_g} t g^2(t)dt \Big/ \int_0^{T_g} g^2(t)dt \tag{41}$$

In summary, if τ_Δ were known, a significant fraction of the energy of $z(t;\hat{\tau},\tau_\Delta)$ would be concentrated in some interval of width W_g around the peak of $g(t)$. In the absence of noise it is easily seen that such an interval would be (t_g, t_g+W_g) with

$$t_g = \arg\max_\alpha \int_\alpha^{\alpha+W_g} g^2(t)dt \tag{42}$$

Now let us consider the case in which τ_Δ lies somewhere within $\hat{\tau}_\Delta \pm \epsilon_\Delta$, where ϵ_Δ is the maximum expected absolute error $|\hat{\tau}_\Delta - \tau_\Delta|$. Inspired by the above arguments we consider the waveform $z(t;\hat{\tau},\tilde{\tau}_\Delta)$, with $\tilde{\tau}_\Delta$ a trial value of τ_Δ. Intuitively, the signal components in $z(t;\hat{\tau},\tilde{\tau}_\Delta)$ are spread over an interval that is broader than W_g, the more so the further $\tilde{\tau}_\Delta$ is from τ_Δ. This suggests estimating τ_Δ by looking for the $\tilde{\tau}_\Delta$ that maximizes the energy of $z(t;\hat{\tau},\tilde{\tau}_\Delta)$ over (t_g, t_g+W_g).

Before proceeding it is interesting to see what happens in the case of two antennas. Here, $z(t;\hat{\tau},\tilde{\tau}_\Delta)$ is proportional to $z_0(t+\hat{\tau}) + z_1(t+\hat{\tau}+\tilde{\tau}_\Delta)$ and its energy is the sum of the separate energies of $z_0(t+\hat{\tau})$ and $z_1(t+\hat{\tau}+\tilde{\tau}_\Delta)$, plus twice the cross-correlation $C(\tilde{\tau}_\Delta)$ between these waveforms. On the other hand the energy of $z_0(t+\hat{\tau})$ is independent of $\tilde{\tau}_\Delta$. Thus, taking the energy of $z_1(t+\hat{\tau}+\tilde{\tau}_\Delta)$ as weakly dependent on $\tilde{\tau}_\Delta$,

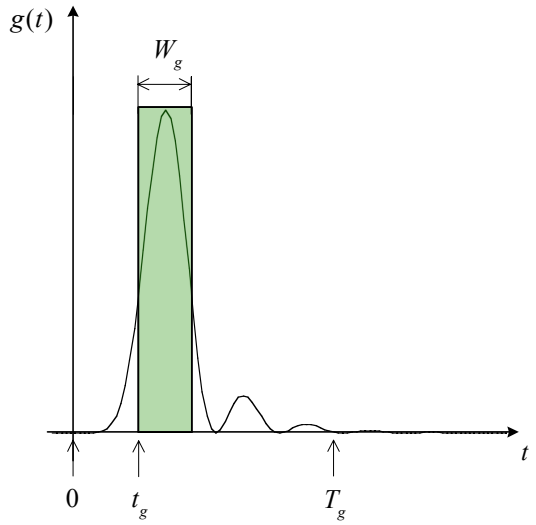

Fig. 5. Shape of pulse $g(t)$ with definitions of T_g and W_g.

it follows that maximizing the energy of $z(t;\hat{\tau},\tilde{\tau}_\Delta)$ amounts to maximizing $C(\tilde{\tau}_\Delta)$. This is reminiscent of the method in [33].

Actually, as the shape of $g(t)$ is unknown and, in consequence, so are t_g and W_g, we replace $(t_g, t_g + W_g)$ with $(\hat{t}_g, \hat{t}_g + \hat{W}_g)$ where $\hat{t}_g$ and $\hat{W}_g$ are approximations of t_g and W_g. This leads to

$$\hat{\tilde{\tau}}_\Delta = \arg\max_{\tilde{\tau}_\Delta} \int_{\hat{t}_g}^{\hat{t}_g+\hat{W}_g} z^2(t;\hat{\tau},\tilde{\tau}_\Delta)dt \tag{43}$$

for $\tilde{\tau}_\Delta$ varying in the interval $(\hat{\tau}_\Delta - \epsilon_\Delta, \hat{\tau}_\Delta + \epsilon_\Delta)$.

What remains to be seen is how $\hat{W}_g$, $\hat{t}_g$ and ϵ_Δ are computed. Starting with $\hat{W}_g$ we consider the waveform $z_0(t)$ corresponding to the antenna with index $n = 0$. From (37) we have

$$z_0(t) = g(t - \tau) + \nu_0(t) \tag{44}$$

which indicates that $z_0(t+\hat{\tau})$ represents a noisy approximation to $g(t)$. This suggests getting $\hat{W}_g$ from (40) and (41) by replacing $g(t)$ with $z_0(t + \hat{\tau})$, i.e.,

$$\hat{W}_g = \sqrt{\int_0^{T_g} (t - \hat{t}_{cg})^2 z_0^2(t+\hat{\tau})dt \Big/ \int_0^{T_g} z_0^2(t+\hat{\tau})dt} \tag{45}$$

with

$$\hat{t}_{cg} = \int_0^{T_g} t z_0^2(t+\hat{\tau})dt \Big/ \int_0^{T_g} z_0^2(t+\hat{\tau})dt \tag{46}$$

With similar arguments $\hat{t}_g$ is derived from (42) as

$$\hat{t}_g = \arg\max_{\alpha} \int_{\alpha}^{\alpha+\hat{W}_g} z_0^2(t+\hat{\tau})dt \tag{47}$$

As for ϵ_Δ, its calculation is carried out in Appendix B with the following result

$$\epsilon_\Delta \cong \begin{cases} \dfrac{3N}{2(N^2-1)} T_N & N \text{ even} \\ \dfrac{3}{2N} T_N & N \text{ odd} \end{cases} \tag{48}$$

Some comments are of interest:

1) The final estimate of θ is obtained from (34) by replacing $\hat{\tau}_\Delta$ with $\hat{\tilde{\tau}}_\Delta$

$$\hat{\hat{\theta}} = \arccos(c\,\hat{\tilde{\tau}}_\Delta / d) \tag{49}$$

2) In deriving (43) we assumed that the continuous-time waveforms $z_n(t)$ are available. As a matter of fact we can only rely on their Nyquist rate samples $z_n(\ell T_N)$. Thus, the previous results must be expressed as a function of these samples. Doing so is straightforward since the $z_n(t)$ can be reconstructed from the $z_n(\ell T_N)$ with an arbitrary resolution T_{os} by cardinal interpolation. Indeed, from the Whittaker-Shannon formula we have

$$z_n(iT_{os}) = \sum_{\ell=-\infty}^{\infty} z_n(\ell T_N) \mathrm{sinc}\left(\frac{iT_{os} - \ell T_N}{T_N}\right), \quad -\infty < i < \infty \tag{50}$$

For a given i, the summation in (50) may be restricted in practice to the samples $z_n(\ell T_N)$ in the interval $(iT_{os} - 6T_N, iT_{os} + 6T_N)$. Details on the expression of $\hat{\tilde{\tau}}_\Delta$ as a function of $z_n(\ell T_N)$ are given in Appendix C.

3) The performance of the estimator $\hat{\tilde{\tau}}_\Delta$ depends on T_{os}. The smaller T_{os} is, the better the performance. On the other hand, the complexity of the estimator increases as T_{os} decreases. Thus, a trade off must be found between accuracy and complexity. We shall return to this point in the next section.

IV. Simulation Results

Computer simulations have been run to assess the performance of the proposed TOA/AOA estimator. Two different monocycles are considered, corresponding to alternative signal spectra and receive filter characteristics. The type-1 monocycle is expressed as $w_1(t) = c_1(t)\cos(2\pi f_0 t)$, where $c_1(t)$ is an 8th order Butterworth pulse with a 3dB bandwidth of 0.75 GHz and f_0 is the center frequency equal to 4 GHz. Pulse $c_1(t)$ is compliant with channels 4, 7, 11 and 15 of [6]. The type-2 monocycle is given by $w_2(t) = c_2(t)\cos(2\pi f_0 t)$, where f_0 is 4.5 GHz and $c_2(t)$ is an 8th order Butterworth pulse with a 3dB bandwidth of 0.25 GHz. Pulse $c_2(t)$ is compliant with channels 0:3, 5:6, 8:10 and 12:14 of [6]. The symbol duration T_s is 200 ns and the observation length K is of 1000 symbols. The channel responses are generated according to model CM1 of [34] and according to [35], [36] for *temporal* and *spatial* characterization, respectively. In particular we use [34] to derive the TOAs and then we assign the AOAs as follows. The angle of arrival of each path is taken from a Laplacian distribution with a standard deviation of 5° and with a mean that varies from cluster to cluster following a uniform distribution in the range $[45^\circ, 135^\circ]$. Also, we imagine that the MS can be anywhere within a rectangular room and the receiver is placed in a corner of the room. The BPFs are ideal rectangular filters with a bandwidth of either 1.5 GHz (with type-1 monocycle) or 0.5 GHz (with type-2 monocycle). Correspondingly, the LPFs are 8th order Butterworth filters with a 3dB bandwidth of 1.5 GHz or 0.5 GHz. The sampling rate at the LPF outputs is either $1/T_N = 3$ GHz or $1/T_N = 1$ GHz. The thermal noise variance σ^2 is assumed known from inter-frame measurements. The

angular position θ of the MS is generated as a uniform random variable in the range $[45°, 135°]$. Finally, the duration of $g(t)$ is approximately $T_g = 2$ ns with type-1 monocycle and $T_g = 6$ ns with type-2 monocycle. It is worth noting that, with these pulse lengths, the assumption we made in Section II that the first path is resolvable is only partially satisfied. Indeed, with the CM1 channel the time separation between first and second path is found to be larger than 2 ns only in 69 percent of the channel realizations, and larger than 6 ns only in 23 percent of the cases. Notwithstanding these discrepancies we shall see that the proposed TOA/AOA estimator has very good performance.

As a performance measure we take the root-mean-squared TOA and AOA estimation errors, RMSE_{TOA} and RMSE_{AOA} respectively. The latter is in degrees while the former is in meters, meaning that the time errors are multiplied by the speed of light. In formulas

$$\mathrm{RMSE}_{TOA} = c \times \sqrt{E\{(\tau - \hat{\tau})^2\}} \tag{51}$$

$$\mathrm{RMSE}_{AOA} = \sqrt{E\{(\theta - \hat{\hat{\theta}})^2\}} \tag{52}$$

where $E\{\cdot\}$ represents average operation. The average is taken over 500 independent channel realizations. Both RMSE_{TOA} and RMSE_{AOA} are given as a function of the ratio E_s/N_0 of the received signal energy per symbol to the noise power spectral density.

Fig. 6 shows the performance of the TOA estimator with two antennas and different values of antenna spacing. As predicted by the theory, the accuracy does not depend on the spacing. The estimation accuracy is excellent with type-1 monocycles. Indeed, an RMSE_{TOA} of 20 cm is obtained with just 10 dB. As expected, the performance is significantly worse with type-2 monocycles since their length is much longer. An RMSE_{TOA} of 20 cm is only achieved at about 45 dB.

Fig. 7 illustrates the corresponding behavior of the AOA estimator. The over-sampling frequency $1/T_{os}$ is 100 GHz and the other parameters are as in Fig. 6. As can be seen, the performance depends on the antenna spacing. At high SNR and with type-1 monocycles the RMSE_{AOA} decreases from about $1.5°$ to $0.4°$ in passing from $d = 25$ cm to $d = 100$ cm. With type-2 monocycles the variation is from $3°$ to $1.5°$.

Fig. 8 and Fig. 9 show the performance of the TOA/AOA estimator as a function of the number of antennas and with an antenna spacing of $d = 25$ cm. The curves in Fig. 8 are virtually overlapped with both type-1 and type-2 monocycles, confirming that RMSE_{TOA} is independent of N. On the other hand the AOA estimation performance improves as N increases, although the gains are marginal for N greater than 3.

Fig. 10 illustrates the influence of the oversampling frequency $1/T_{os}$ on the AOA estimator performance. The array has two antennas at a distance of 50 cm and E_s/N_0 is 20 dB. With type-1 monocycles the RMSE_{AOA} decreases steadily as $1/T_{os}$ increases until about 60 GHz. No further improvement is observed beyond 60 GHz. With type-2 monocycles the best performance is already achieved at 20 GHz.

Fig. 11 and Fig. 12 make comparisons with the TOA/AOA estimator in [30] and with the Cramer-Rao bounds (CRBs) as obtained with the approach in [24]. The number of antennas

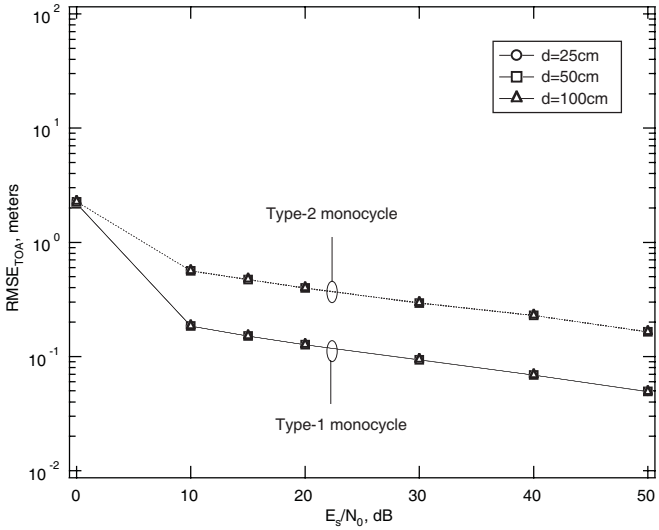

Fig. 6. RMSE_{TOA} in meters vs. E_s/N_0 with $N = 2$ antennas and $d = 25$, 50 or 100 cm.

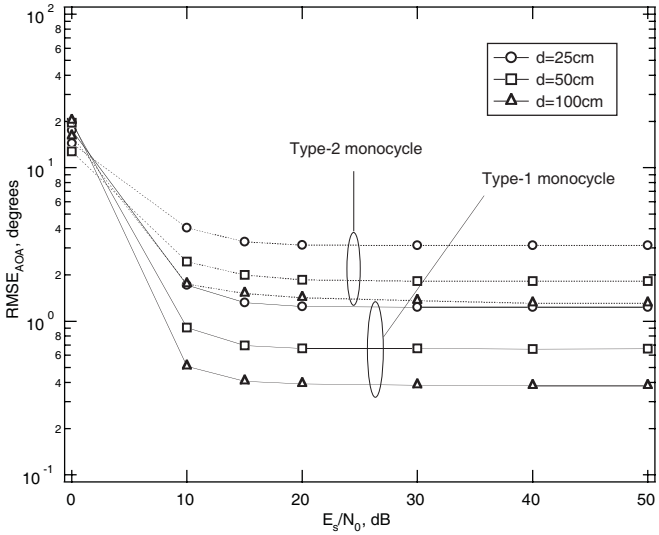

Fig. 7. RMSE_{AOA} in degrees vs. E_s/N_0 with $N = 2$ antennas and $d = 25$, 50 or 100 cm. The over-sampling frequency $1/T_{os}$ is 100 GHz.

is $N = 2$, with a spacing of 50 cm. Either type-1 or type-2 monocycles are used. The scheme in [30] operates in two steps. In the first step the signal $x_n(t)$ from the BPF at the nth antenna is sampled at Nyquist rate $1/T'_N$. Next, the time-domain sequence $\{x_n(\ell T'_N)\}$ is fed to a Discrete Fourier Transform unit that produces frequency-domain samples with spacing $1/T'_N$. Finally, the frequency-domain samples are processed to get an estimate $\hat{\tau}_n$ of the propagation delay τ_n. In the second step, the best linear unbiased estimator of TOA and AOA is derived from the $\hat{\tau}_n$. It should be noted that, as the samples in [30] are taken at the BPF outputs while in our estimator they are taken at the LPF outputs, the sampling rate $1/T'_N$ is much higher than $1/T_N$. Indeed, with the system parameters previously chosen, we have $1/T'_N = 10$ GHz with both type-1 and type-2 monocycles whereas $1/T_N$ is 3 GHz in the first case and 1 GHz in the second case. This decrease in sampling rate translates into a reduction

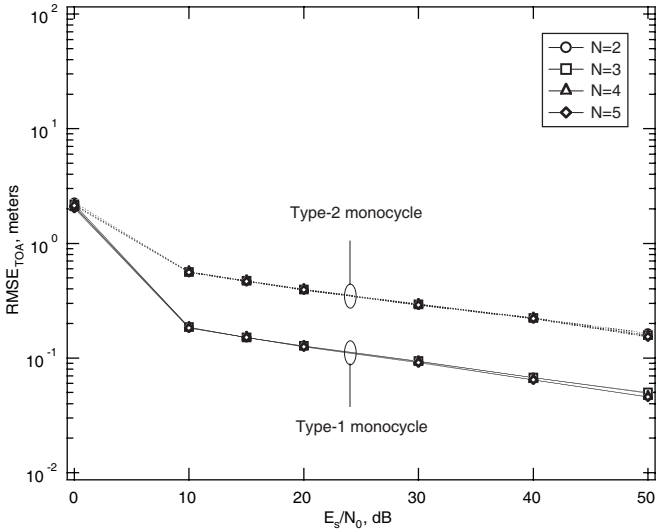

Fig. 8. RMSE_{TOA} in meters vs. E_s/N_0 with 2, 3, 4 or 5 antennas. The distance d is 25 cm.

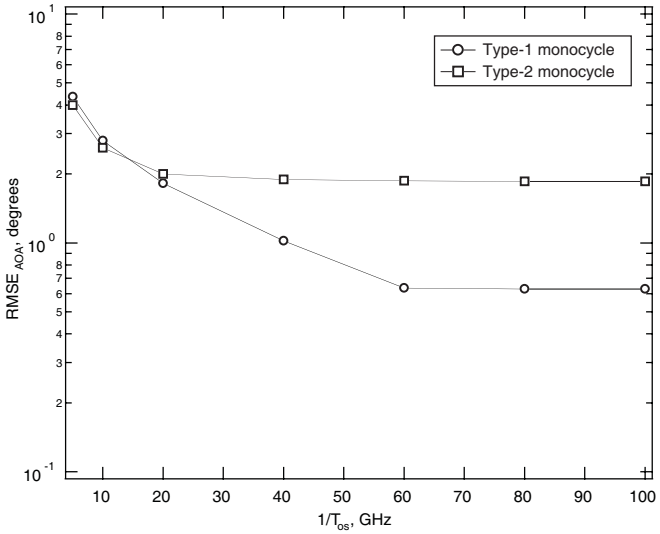

Fig. 10. RMSE_{AOA} in degrees vs. $1/T_{os}$. The number of antennas is $N = 2$, $d = 50$ cm and $E_s/N_0 = 20$ dB.

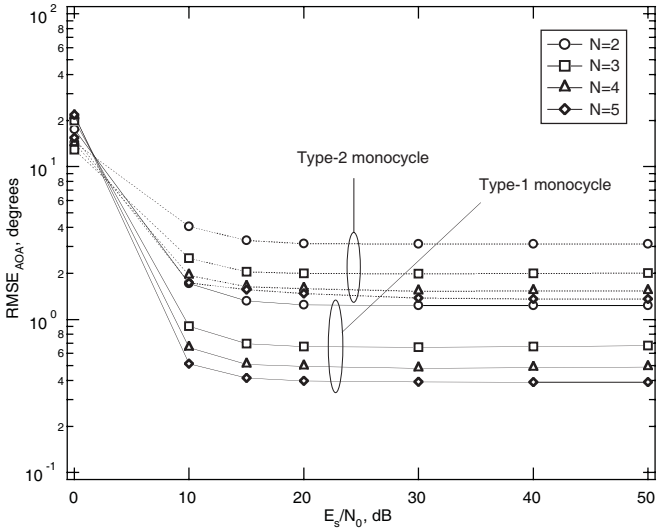

Fig. 9. RMSE_{AOA} in degrees vs. E_s/N_0 with 2, 3, 4 or 5 antennas. The distance d is 25 cm.

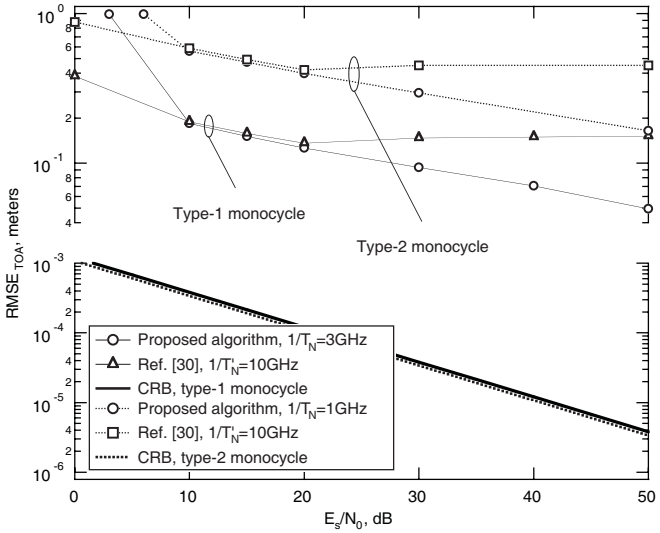

Fig. 11. Comparison between the proposed TOA estimator and that in [30]. The array has two antennas at a distance of 50 cm. Both type-1 and type-2 monocycles are considered.

by a factor T'_N/T_N (see [37]) of the power consumption in the receiver's analog-to-digital converters. Alternatively, with the same power consumption, it allows us to increase their resolution by about $\log_2(T_N/T'_N)$ bits. For example, with type-2 monocycles the power consumption is reduced by one order of magnitude while the resolution is increased by 3 bits.

As far as the performance is concerned, Fig. 11 indicates that the proposed TOA estimator is comparable or slightly better than that in [30] at SNR of practical interest. On the other hand Fig. 12 shows that the proposed AOA estimator is superior to the one in [30] at any SNR.

Some more details regarding Fig. 11 are needed because the large gap between the CRBs and the actual TOA errors might suggest that other estimators with much better performance exist. In this regard it is worth pointing out the following: First, a comparable gap is shown in Fig. 5 of [9] illustrating the performance of a threshold-based TOA estimator with a single antenna. Secondly, the CRBs are computed assuming perfect knowledge of the shape of the received pulses, which is far from being realistic. Finally, those in Fig. 11 are not true CRBs but only optimistic approximations. Indeed, as in [9] and [24], they have been computed assuming that the first path is resolvable. Thus, all the other paths can be eliminated and the multipath signal may be thought of as equivalent to a signal with only the first path as far as TOA measurements are concerned.

V. Conclusion

A joint TOA/AOA estimator has been proposed for accurate indoor UWB localization applications. The device employs an array of antennas, each feeding a demodulator consisting of a squarer and a low-pass filter. The signal samples from the filter outputs are processed to produce TOA and AOA

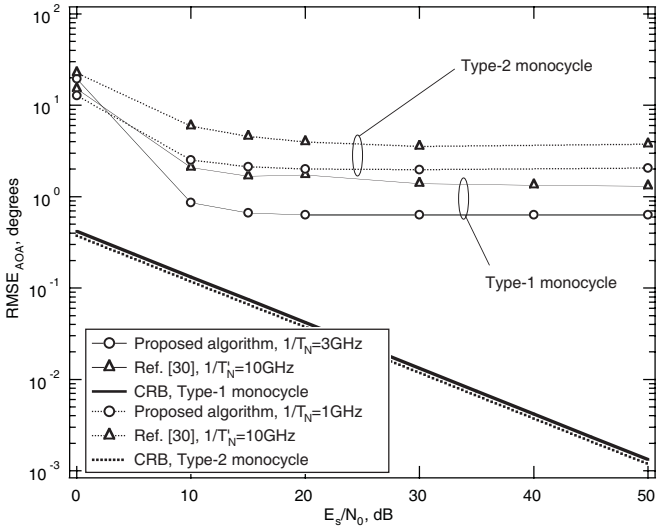

Fig. 12. Comparison between the proposed AOA estimator and that in [30]. The array has two antennas at a distance of 50 cm. Both type-1 and type-2 monocycles are considered.

estimates. Simulations have been run assuming transmitted pulses with a bandwidth of either 0.5 GHz (type-2 pulses) or 1.5 GHz (type-1 pulses), requiring sampling rates of 1 GHz and 3 GHz, respectively. Ranging accuracies of about 20 cm and angular accuracies of about 0.8° are achieved at SNR of practical interest with type-1 pulses and two antennas at a distance of 50 cm. Some degradations are incurred with type-2 pulses. The performance of the joint estimator has been compared with that of another scheme proposed in literature. Advantages in terms of performance and power consumption have been pointed out.

APPENDIX A
COMPUTATION OF MSE_θ

We start from (34), writing $\hat{\tau}_\Delta$ as the sum of τ_Δ plus some error ϵ_{τ_Δ}

$$\hat{\theta} = \arccos\left[\frac{c}{d} \times (\tau_\Delta + \epsilon_{\tau_\Delta})\right] \tag{53}$$

Expanding the RHS into a Taylor's series truncated to the second term results in

$$\hat{\theta} \cong \arccos(c\,\tau_\Delta/d) - \frac{c\,\epsilon_{\tau_\Delta}}{d\sin\theta} \tag{54}$$

On the other hand, from (6) we have $\arccos(c\,\tau_\Delta/d) = \theta$ so that (54) becomes

$$\hat{\theta} - \theta \cong -\frac{c\,\epsilon_{\tau_\Delta}}{d\sin\theta} \tag{55}$$

from which the mean-squared value of $\hat{\theta} - \theta$ conditioned on θ is found to be

$$\mathrm{MSE}_\theta(\theta) = \frac{c^2}{d^2} \times \frac{1}{\sin^2\theta} \times \mathrm{MSE}_{\tau_\Delta} \tag{56}$$

Averaging the RHS over the interval $\theta_1 \le \theta \le \theta_2$ provides the unconditional mean-squared error MSE_θ as given in (35).

APPENDIX B
COMPUTATION OF ϵ_Δ

The value of ϵ_Δ is computed as follows. Substituting (25) into (30) one gets

$$\hat{\tau}_\Delta = \tau_\Delta + \frac{12}{N\left(N^2-1\right)} \sum_{n=0}^{N-1} \left(n - \frac{N-1}{2}\right)(u_n + \delta_{th,n}) \tag{57}$$

Now, assume the SNR high enough so that $\delta_{th,n}$ can be neglected compared to u_n (by simulation it is found that this condition is satisfied for $E_s/N_0 > 20$ dB). Then (57) becomes

$$\hat{\tau}_\Delta = \tau_\Delta + \frac{12}{N\left(N^2-1\right)} \sum_{n=0}^{N-1} \left(n - \frac{N-1}{2}\right) u_n \tag{58}$$

from which, bearing in mind that $u_n \in [-T_N/2, T_N/2)$, it follows

$$\begin{aligned} |\hat{\tau}_\Delta - \tau_\Delta| &\le \frac{12}{N\left(N^2-1\right)} \sum_{n=0}^{N-1} \left|\left(n - \frac{N-1}{2}\right)\right| |u_n| \\ &\le \frac{6T_N}{N\left(N^2-1\right)} \sum_{n=0}^{N-1} \left|\left(n - \frac{N-1}{2}\right)\right| \\ &= \begin{cases} 3NT_N/2(N^2-1) & N \text{ even} \\ 3T_N/2N & N \text{ odd} \end{cases} \end{aligned} \tag{59}$$

Thus,

$$\epsilon_\Delta \triangleq \max|\hat{\tau}_\Delta - \tau_\Delta| = \begin{cases} \dfrac{3N}{2(N^2-1)} T_N & N \text{ even} \\ \dfrac{3}{2N} T_N & N \text{ odd} \end{cases} \tag{60}$$

APPENDIX C
DIGITAL IMPLEMENTATION OF THE AOA ESTIMATOR

To describe the digital implementation of the improved AOA estimator we start from the samples $z_n(\ell T_{os})$ in (50). Letting $M_g \triangleq \lfloor T_g/T_{os} \rfloor$ and $m_\tau \triangleq \lfloor \hat{\tau}/T_{os} \rfloor$, we first compute a discrete-time approximation of $\hat{W}_g$ in the form $M_W T_{os}$, where M_W is the integer part of

$$\frac{1}{T_{os}} \sqrt{\frac{\sum_{\ell=0}^{M_g-1} \left(\ell T_{os} - \bar{t}_{cg}\right)^2 z_0^2\left(\ell T_{os} + m_\tau T_{os}\right)}{\sum_{\ell=0}^{M_g-1} z_0^2\left(\ell T_{os} + m_\tau T_{os}\right)}} \tag{61}$$

and

$$\bar{t}_{cg} \triangleq \frac{\sum_{\ell=0}^{M_g-1} \ell T_{os} z_0^2\left(\ell T_{os} + m_\tau T_{os}\right)}{\sum_{\ell=0}^{M_g-1} z_0^2\left(\ell T_{os} + m_\tau T_{os}\right)} \tag{62}$$

Next, a discrete-time approximation of $\hat{t}_g$ is obtained in the form $m_g T_{os}$, with

$$m_g = \arg\max_{\tilde{m}_g} \sum_{\ell=\tilde{m}_g}^{\tilde{m}_g+M_W} z_0^2\left(\ell T_{os} + m_\tau T_{os}\right) \tag{63}$$

Then, taking $\tilde{\tau}_\Delta = \tilde{m}_\Delta T_{os}$ with $\tilde{m}_\Delta$ an integer, the digital version of (43) reads

$$m_\Delta = \arg\max_{\tilde{m}_\Delta} \sum_{\ell=m_g}^{m_g+M_W} z^2\left(\ell T_{os}; m_\tau T_{os}, \tilde{m}_\Delta\right) \tag{64}$$

with

$$z\left(\ell T_{os}; m_\tau T_{os}, \tilde{m}_\Delta\right) \triangleq \frac{1}{N}\sum_{n=0}^{N-1} z_n\left(\ell T_{os} + m_\tau T_{os} + n\tilde{m}_\Delta T_{os}\right) \tag{65}$$

and the final estimate of τ_Δ becomes $\hat{\tilde{\tau}}_\Delta = m_\Delta T_{os}$.

REFERENCES

[1] S. Gezici, Z. Tian, G. B. Giannakis, H. Kobayashi, A. F. Molish, H. V. Poor, and Z. Sahinoglu, "Localization via ultra-wideband radios," *IEEE Signal Process. Mag.*, vol. 22, no. 4, pp. 70–84, July 2005.

[2] L. Yang and G. B. Giannakis, "Ultra-wideband communications: an idea whose time has come," *IEEE Signal Process. Mag.*, vol. 21, pp. 26–54, Nov. 2004.

[3] R. Knochel, A. Gulck, F. Daschner, and O. Schimmer, "UWB-sensors for industrial applications," in *IEEE Int. Conf. UWB*, 2007.

[4] F. Althaus, F. Chin, J. Kunisch, J. Pamp, and B. e. a. Radunovic, "A comprehensive investigation of UWB sensor networks for industrial applications," in *IST Mobile Wireless Comm. Summit*, 2006.

[5] S. Colson and H. Hoff, "Ultra-wideband technology for defence applications," in *Proc. IEEE International Conference on ICU*, Sep. 2005, pp. 615–620.

[6] IEEE Standard 802.15.4a-2007 Task Group, "Part 15.4: wireless medium access control (MAC) and physical layer (PHY) specifications for low-rate wireless personal area networks (WPANs)," tech. rep., Mar. 2007.

[7] J.-Y. Lee and R. A. Scholtz, "Ranging in a dense multipath environment using an UWB radio link," *IEEE Trans. Sel. Areas Commun.*, vol. 20, no. 9, pp. 1677–1683, Dec. 2002.

[8] D. Dardari, A. Conti, U. Ferner, A. Giorgetti, and M. Win, "Ranging with ultrawide bandwidth signals in multipath environments," *Proc. IEEE*, vol. 97, no. 2, pp. 404–426, Feb. 2009.

[9] D. Dardari, C.-C. Chong, and M. Win, "Threshold-based time-of-arrival estimators in UWB dense multipath channels," *IEEE Trans. Commun.*, vol. 56, no. 8, pp. 1366–1378, Aug. 2008.

[10] S. Gezici, Z. Sahinoglu, A. F. Molish, H. Kobayashi, and H. V. Poor, "A two-step time of arrival estimation algorithm for impulse radio ultra wideband systems," in *Proc. 13th European Signal Processing Conference*, Sep. 2005.

[11] I. Guvenc and Z. Sahinoglu, "Threshold-based TOA estimation for impulse radio UWB systems," in *Proc. IEEE Int. Conf. on UWB*, Sep. 2005, pp. 420–425.

[12] A. A. D'Amico, U. Mengali, and L. Taponecco, "TOA estimation with the IEEE 802.15.4a standard," *IEEE Trans. Wireless Commun.*, vol. 9, pp. 2238–2247, Sep. 2010.

[13] C. Falsi, D. Dardari, L. Mucchi, and M. Win, "Time of arrival estimation for UWB localizers in realistic environments," *EURASIP J. Applied Signal Process.*, vol. 2006, Nov. 2010.

[14] D. Dardari, C.-C. Chong, and M. Z. Win, "Improved lower bounds on time-of-arrival estimation error in realistic UWB channels," in *Proc. IEEE International Conference on Ultra-Wideband*, Sep. 2006.

[15] J. Ni, D. Arndt, P. Ngo, C. Phan, and J. Gross, "Ultra-wideband two-cluster tracking system design with angle of arrival algorithm," in *Proc. IEEE Conference on Radar*, vol. 6, Apr. 2006, pp. 24–27.

[16] Y. Luo and C. L. Law, "UWB indoor positioning based on uniform circular antenna array," in *Proc. 11th IEEE Singapore International Conference on Communication Systems*, Nov. 2008, pp. 138–142.

[17] L. Pierucci and P. Roig, "UWB localization on indoor MIMO channels," in *Proc. International Conference on Wireless Networks, Communications and Mobile Computing*, vol. 2, June 2005, pp. 890–894.

[18] J. Xu, M. Ma, and C. L. Law, "AOA cooperative position localization," in *Proc. IEEE Global Telecommunications Conference*, Dec. 2008, pp. 1–5.

[19] L. Cong and W. Zhuang, "Nonline-of-sight error mitigation in mobile location," *IEEE Trans. Wireless Commun.*, vol. 4, no. 2, pp. 560–573, Mar. 2005.

[20] I. Guvenc, C.-C. Chong, F. Watanabe, and H. Inamura, "NLOS identification and weighted least-squares localization for UWB systems using multipath channel statistics," *EURASIP J. Advances Signal Process.*, vol. ID 271984, 2008.

[21] L. Xiong, "A selective model to suppress NLOS signals in angle-of-arrival (AOA) location estimation," in *Proc. IEEE International Symposium on Personal, Indoor and Mobile Radio Communications*, Sep. 1998, pp. 461–465.

[22] R. J. Fontana, E. Richley, and J. A. Barney, "Commercialization of an ultra wideband precision asset location system," in *IEEE Conference on Ultra Wideband Systems and Technologies*, Nov. 2003.

[23] A. Mallat, J. Louveaux, and L. Vandendorpe, "UWB based positioning: Cramer-Rao bound for angle of arrival and comparison with time of arrival," in *Proc. 13th Symposium on Communications and Vehicular Technology*, vol. 3, Nov. 2006.

[24] ——, "UWB based positioning in multipath channels: CRBs for AOA and for hybrid TOA-AOA based methods," in *Proc. IEEE International Conference on Communications*, June 2007, pp. 5775–5780.

[25] T. Kleine-Ostmann and A. Bell, "A data fusion architecture for enhanced position estimation in wireless networks," *IEEE Commun. Lett.*, vol. 5, no. 8, pp. 343–345, Aug. 2001.

[26] L. Cong and W. Zhuang, "Hybrid TDOA/AOA mobile user location for wideband CDMA cellular systems," *IEEE Trans. Wireless Commun.*, vol. 1, no. 3, pp. 439–447, July 2002.

[27] N. Thomas, D. Cruickshank, and D. Laurenson, "Performance of a TDOA-AOA hybrid mobile location system," in *Proc. Second International Conference on 3G Mobile Communication Technologies*, 2001, pp. 216–220.

[28] P. Deng and P. Fan, "An AOA assisted TOA positioning system," in *Proc. International Conference on Communication Technology*, vol. 2, 2000, pp. 1501–1504.

[29] S. Galler, W. Gerok, J. Schroeder, K. Kyamakya, and T. Kaiser, "Combined AOA/TOA UWB localization," in *Proc. International Symposium on Communications and Information Technologies*, Oct. 2007, pp. 1049–1053.

[30] M. Navarro and M. Najar, "Joint estimation of TOA and DOA in IR-UWB," in *Proc. IEEE 8th Workshop on Signal Processing Advances in Wireless Communications*, June 2007, pp. 1–5.

[31] M. K. Simon, *Probability Distributions Involving Gaussian Random Variables*. Kluwer Academic Publishers, 2002.

[32] S. M. Kay, *Fundamentals of Statistical Signal Processing: Estimation Theory*. Prentice-Hall, Inc., 1993.

[33] J. Chen, J. Benesty, and Y. Huang, "Time delay estimation in room acoustic environments: an overview," *EURASIP J. Applied Signal Process.*, vol. 2006, pp. 1–19, Jan. 2006.

[34] A. F. Molisch, K. Balakrishnan, C.-C. Chong, S. Emami, A. Fort, J. Karedal, H. Schantz, U. Schuster, and K. Siwiak, "IEEE 802.15.4a channel model-final report," tech. rep., Feb. 2005.

[35] S. Venkatesh, V. Bharadwaj, and R. Buehrer, "A new spatial model for impulse-based ultra-wideband channels," in *Proc. IEEE Vehicular Technology Conference-Fall*, vol. 4, Sep. 2005, pp. 2617–2621.

[36] R.-M. Cramer, R. Scholtz, and M. Win, "Evaluation of an ultra-wideband propagation channel," *IEEE Trans. Antennas Propag.*, vol. 50, no. 5, pp. 561–570, May 2002.

[37] R. H. Walden, "Analog-to-digital converter survey and analysis," *IEEE J. Sel. Areas Commun.*, vol. 17, no. 4, pp. 539–550, Apr. 1999.

Antonio A. D'Amico received the Dr. Ing. Degree in Electronic Engineering in 1992 and the Ph. D. degree in 1997, both from the University of Pisa, Italy. He is currently a Research Fellow at the Department of Information Engineering of the University of Pisa. His research interests are in digital communication theory, with emphasis on synchronization algorithms, channel estimation and detection techniques.

Umberto Mengali (M69-SM85-F90) received his education in Electrical Engineering from the University of Pisa. In 1971 he obtained the Libera Docenza in Telecommunications from the Italian Education Ministry. Since 1963 he has been with the Department of Information Engineering of the University of Pisa where he is a Professor of Telecommunications. In 1994 he was a Visiting Professor at the University of Canterbury, New Zealand as an Erskine Fellow. He has served in the technical program committee of several international conferences and has been technical Co-Chair of the 2004 International Symposium on Information Theory and Applications (ISITA). His research interests are in digital communications and communication theory, with emphasis on synchronization methods and modulation techniques. He has co-authored the book *Synchronization Techniques for Digital Receivers* (Plenum Press, 1997). Professor Mengali is a member of the Communication Theory Committee and has been an editor of the IEEE TRANSACTIONS ON COMMUNICATIONS from 1985 to 1991 and of the *European Transactions on Telecommunications* from 1997 to 2000.

Lorenzo Taponecco received the Dr. Ing. degree (cum laude) in Telecommunications Engineering in 2002 and the Ph.D. degree in Information Engineering in 2007, both from the University of Pisa, Pisa, Italy. Since 2007, he has been with the Department of Information Engineering at the University of Pisa where he is currently a Research Assistant of telecommunications. His research interests include the area of digital communication theory, with special emphasis on ultrawideband (UWB) communications, parameter estimation, synchronization and localization techniques.